ChemPubSoc Europe

DOI: 10.1002/chem.201505107

CHEMISTRY A European Journal Full Paper

Metal–Organic Frameworks

Extraordinary Separation of Acetylene-Containing Mixtures with Microporous Metal–Organic Frameworks with Open O Donor Sites and Tunable Robustness through Control of the Helical Chain Secondary Building Units

Zizhu Yao,[a] Zhangjing Zhang,[a] Lizhen Liu,[a] Ziyin Li,[a] Wei Zhou,[b] Yunfeng Zhao,[c, f] Yu Han,[c] Banglin Chen,[d] Rajamani Krishna,*[e] and Shengchang Xiang*[a]

Abstract: Acetylene separation is a very important but challenging industrial separation task. Here, through the solvothermal reaction of CuI and 5-triazole isophthalic acid in different solvents, two metal–organic frameworks (MOFs, **FJU-21** and **FJU-22**) with open O donor sites and controllable robustness have been obtained for acetylene separation. They contain the same paddle-wheel $\{Cu_2(COO_2)_4\}$ nodes and metal–ligand connection modes, but with different helical chains as secondary building units (SBUs), leading to different structural robustness for the MOFs. **FJU-21** and **FJU-22** are the first examples in which the MOFs' robustness is controlled by adjusting the helical chain SBUs. Good robustness gives the activated **FJU-22a**, which has higher surface area and gas uptakes than the flexible **FJU-21a**. Importantly, FJU-22a shows extraordinary separation of acetylene mixtures under ambient conditions. The separation capacity of **FJU-22a** for 50:50 C_2H_2/CO_2 mixtures is about twice that of the high-capacity HOF-3, and its actual separation selectivity for C_2H_2/C_2H_4 mixtures containing 1% acetylene is the highest among reported porous materials. Based on first-principles calculations, the extraordinary separation performance of C_2H_2 for **FJU-22a** was attributed to hydrogen-bonding interactions between the C_2H_2 molecules with the open O donors on the wall, which provide better recognition ability for C_2H_2 than other functional sites, including open metal sites and amino groups.

Introduction

Removal of acetylene from C_2H_2/C_2H_4 mixtures is an important and highly challenging industrial process.[1–5] Ethylene, the largest volume organic chemical, is widely used for the production of polymers. Ethylene produced in steam crackers typically contains on the order of 1% of acetylene,[6] which should be reduced to an accepted level in the ethylene feed before polymerization, because acetylene can poison Ziegler–Natta catalysts and also lower the resulting product quality.[7] Current approaches to remove acetylene include partial hydrogenation over a noble metal catalyst[8] and the solvent extraction of cracked olefins,[9] but both of these are cost and energy consumptive.

The emerging microporous metal–organic frameworks (MOFs)[10–13] based on physical adsorption are promising as cost-effective and efficient materials for gas separation, which has been a topic of interest because the ability to rationally design and chemically tune their architecture of the MOFs allows chemists to establish various methods to achieve highly selective gas adsorption.[10–29] Since the pioneered work of Kitagawa and co-workers,[14] some MOFs with high acetylene storage have been realized by using immobilized open metal sites (OMS).[30,31] For C_2H_2/C_2H_4 separation, after the first work realized by using the flexible MOFs on the basis of metalloligands in 2011,[2] the series of MOF-74[3] with high densities of open

[a] Z. Yao, Prof. Dr. Z. Zhang, L. Liu, Z. Li, Prof. Dr. S. Xiang
Fujian Provincial Key Laboratory of Polymer Materials
Fujian Normal University, 32 Shangsan Road
Fuzhou 350007 (P. R. China)
E-mail: scxiang@fjnu.edu.cn

[b] Prof. Dr. W. Zhou
NIST Center for Neutron Research, Gaithersburg
Maryland 20899-6102 (USA)

[c] Dr. Y. Zhao, Prof. Dr. Y. Han
Advanced Membranes and Porous Materials Center
Physical Sciences and Engineering Division
King Abdullah University of Science and Technology
Thuwal 23955-6900 (Saudi Arabia)

[d] Prof. Dr. B. Chen
Department of Chemistry, University of Texas at San Antonio
One UTSA Circle, San Antonio, Texas 78249-0698 (USA)

[e] Prof. Dr. R. Krishna
Van't Hoff Institute for Molecular Sciences, University of Amsterdam
Science Park 904
Amsterdam 1098 XH (The Netherlands)

[f] Dr. Y. Zhao
Institute for New Energy Materials & Low-Carbon Technologies
School of Materials Science and Engineering
Tianjin University of Technology, Tianjin 300384 (P. R. China)

Supporting information and ORCID for the author for this article are available on the WWW under http://dx.doi.org/10.1002/chem.201505107.

metal sites and NOTT-300[4] with multiple weak supramolecular interactions were also employed. However, these three kinds of MOFs are not the ideal materials; the former exhibit very low acetylene uptake and the latter two show very low selectivity toward acetylene. A recent MOF, UTSA-100, containing amino groups[5] is a unique example for actual column breakthrough experiments of C_2H_2/C_2H_4 mixtures, giving moderate selectivity and moderate acetylene uptake. Additionally, owing to the similar fluid properties of acetylene and CO_2, the efficient separation of C_2H_2/CO_2 mixture is another technologically interesting issue.[14,28] A few MOFs and zeolites with relevant differences in capacity for C_2H_2/CO_2 have been developed, mainly through tuning the cross-section size of the pore.[32] To date, no MOFs or other porous materials have been found with actual C_2H_2/CO_2 breakthrough experiments, except one hydrogen-bonded organic framework (HOF-3),[33] however, this has low separation capacity. The MOFs for the separation of C_2H_2 mixtures have not been fully explored. It is still desirable to explore new ways to construct the MOFs with excellent performance for the challenging separations of C_2H_2/CO_2 and C_2H_2/C_2H_4 mixtures.

In this work, through solvothermal reactions of 5-triazole isophthalic acid (H_2L), CuI, and various solvents, two MOFs $\{[Cu(L)](DMF)(H_2O)_{1.5}\}_n$ (**FJU-21**, DMF = *N*,*N*′-dimethylformamide) and $\{[Cu(L)]\cdot(DMA)(H_2O)_{1.5}\}_n$ (**FJU-22**, DMA = *N*,*N*′-dimethylacetamide) with open O donor sites and controllable robustness have been obtained for the highly selective separation of both C_2H_2/CO_2 and C_2H_2/C_2H_4 mixtures. This was done on the base of the following considerations. (1) The remarkable difference between C_2H_2 and other gases including CO_2 and ethylene is the acidic hydrogen atoms at both ends of acetylene. Thus, the different framework flexibilities, different OMS and amino groups, and the open O donors can endow the MOFs with exclusive recognition ability for C_2H_2 through extra hydrogen-bonding interactions. (2) The use of 5-triazole isophthalic acid (H_2L) containing one heterocyclic and two carboxylate groups to construct the MOFs may generate rich open O donor sites (without H riding) standing on the framework wall to recognize acetylene. (3) Solvent-induced structure diversity with controllable robustness may be observed to further control the acetylene separation capacity. As expected, the open O donors can provide the MOFs better recognition ability for C_2H_2 than other functional sites, including the OMS and amino groups. The activated **FJU-22a** with open O donors and good robustness exhibits extraordinary separation performances for both C_2H_2/CO_2 and C_2H_2/C_2H_4 mixtures at ambient conditions as demonstrated by gas adsorption, breakthrough simulations, actual column breakthrough experiments, and first-principles calculations.

Results and Discussion

Solvent-induced structure diversity

Green needle-like crystals of **FJU-21** could be obtained in DMF/H_2O (3:2, v/v) mixed solvent at 85 °C for 1 day, and bulk crystals of **FJU-22** could be obtained by the same method

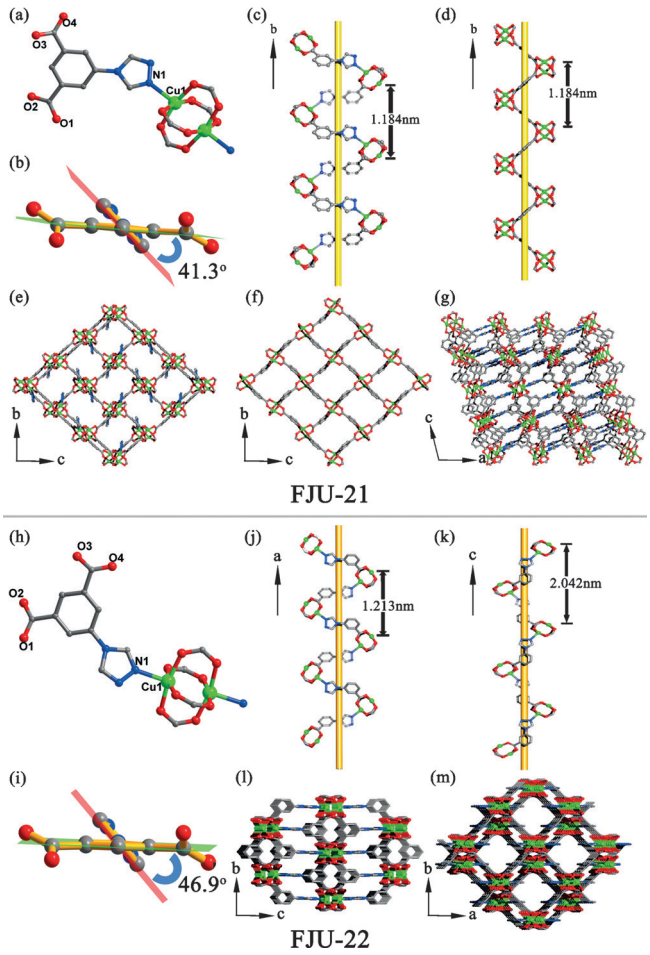

Figure 1. The structures of **FJU-21** (a–g) and **FJU-22** (h–m) showing: the coordination environment of **FJU-21** (a) and **FJU-22** (h); the twist angle between the triazole ring and the plane of the benzene ring of the ligand in **FJU-21** (b) and **FJU-22** (i); the two kinds of helical chain SBUs of **FJU-21** (c and d) along the *b* axis; the unique kind of helical chain SBUs with various pitches along the *a* and *c* axes in **FJU-22** (j and k); the triazole-pillared [Cu_2(isophthalate)$_4$] bilayers in the orientation of the (200) plane of **FJU-21** (e); the [Cu_2(isophthalate)$_4$] monolayers in the orientation of the (100) plane of **FJU-21** (f); 3D framework of **FJU-21** along the *b* axis (g); and 3D framework of **FJU-22** view along the *a* and *c* axes (l and m). Color code: Cu, green; C, gray; O, red; N, blue.

except that DMF was replaced by DMA. Single-crystal X-ray diffraction analyses reveal that **FJU-21** and **FJU-22** have the same metal nodes and metal–ligand connection modes (Figure 1). In each crystallographically independent unit, there is one Cu^{II} ion and one ligand. The Cu^{II} ion is fivefold coordinated by four oxygen atoms and one triazolyl N donor from five ligands and has a square-pyramidal coordination environment. Two Cu^{II} ions are bridged by four carboxylate groups to give a paddle-wheel node (PWN). The axial site of the PWN is occupied by triazolyl N donors. The ligand L employs its one triazole N and four carboxylate O atoms to link three PWNs. In **FJU-22**, the twist angle between the triazole ring and the plane of the benzene ring of the ligand L (46.9°) is higher than that of **FJU-21** (41.3°), as shown in Figure 1i and b. The non-planarity of ligand L with various twist angles endows the two MOFs with various helical chains that act as secondary building units

(SBUs). **FJU-22** has a unique type of helical chain SBU with different pitches composed of the PWNs and *N*-benzene triazole linkers along the *a* and *c* axes (Figure 1j and k). The linkage between adjacent SBUs sharing the PWNs results in a three-dimensional (3D) skeleton (Figure 1l and m). **FJU-21** has two types of helical chain SBUs along the *b* axis. One has the same composites as that in **FJU-22** (Figure 1c), which connects with the neighboring SBUs to give triazole-pillared $[Cu_2(isophthalate)_4]$ bilayers in the orientation of the (200) plane (Figure 1e), whereas the other is made up of the PWNs and isophthalate linkers (Figure 1d), and connects with the adjacent SBUs to produce $[Cu_2(isophthalate)_4]$ monolayers oriented at the (100) plane (Figure 1f). The bilayers and monolayers stack on each other by layer-sharing along the *a* axis to form the 3D framework (Figure 1g). By considering the PWN as a six-connected octahedral node and the ligand as a three-connected trigonal linker, the whole frameworks of **FJU-21** and **FJU-22** can be simplified to a (3,6)-connected net with rutile (rtl) and α-PbO_2 (apo) topology, respectively. **FJU-21** shows a 1D channel along the *a* axis (5.00×9.60 Å^2), whereas **FJU-22** also has a 1D channel, but along the *c* axis (7.10×7.10 Å^2; Figure S1 in the Supporting Information). PLATON calculations[34,35] of **FJU-21** and **FJU-22** indicate their void volumes are 923.7 Å^3 (52.1% of the unit cell volume of 1773.3 Å^3) and 1908 Å^3 (52.8% of the unit cell volume of 3614.2 Å^3), respectively.

Owing to the same metal node and metal–ligand connection mode, **FJU-21** and **FJU-22** have similar pore surface structures. Nevertheless, it is worth noting that the solvent-induced structural diversity gives the two MOFs distinct robustness properties. The two as-synthesized MOFs were exchanged with CH_3OH and CH_2Cl_2, respectively, several times, then heated to 60 °C, and evacuated under high vacuum to obtain the desolvated frameworks **FJU-21a** and **FJU-22a.** **FJU-21a** is flexible, whereas **FJU-22a** shows good robustness, as proved by powder X-ray diffraction experiments (PXRD; Figure S2 in the Supporting Information). For **FJU-22**, with the one unique type of helical chain SBU, the 2θ values are not shifted for the activated sample compared to the as-synthesized sample pattern. However, for **FJU-21**, which contains one more type of helical chain SBU, the values of 2θ for the (100) and (002) planes are shifted to higher angles for the activated sample, and no shift for the (020) plane is seen, indicating that the dynamic features are down to the $[Cu_2(isophthalate)_4]$ monolayers oriented at the (100) plane and constructed from the helical chains exclusively in **FJU-21** and not observed in **FJU-22**. In addition, if exposed to air or water vapor, the values of 2θ for **FJU-21** are shifted, whereas for **FJU-22** there is no obvious change under the same conditions, further indicating that **FJU-22** has better stability than **FJU-21**. Although several methods including those using high-valent metal ions,[36] modulated synthesis,[37] N-donor ligands,[38] and superhydrophobic ligands[39] have been proposed to enhance MOF stability, **FJU-21** and **FJU-22** are the first examples to demonstrate control of MOF stability and robustness by adjusting the helical chain SBUs.

Gas adsorption

To assess the permanent porosity, the N_2 sorption isotherms of the activated **FJU-21a** and **FJU-22a** materials were examined at 77 K (Figure 2), which yielded a reversible type I isotherm for the microporous nature of the samples with Brunauer–Emmett–Teller (BET) surface areas of 369.10 and 828.19 m^2g^{-1}, respectively. **FJU-21a** shows a bimodal pore size distribution centered at 5.2 and 8.7 Å, and **FJU-22a** has a distribution centered at 8.0 Å, as calculated by the non-local (NL)-DFT method; these values are close to the pore sizes determined from the crystal structures (Figure S1 in the Supporting Information). Although their void volumes from the Platon calculations are close, the BET surface area for **FJU-21a**, with the dynamic framework, is only about half that for **FJU-22a**. The flexible character of **FJU-21** is further confirmed by a hysteresis loop in the N_2 adsorption isotherm at 77 K.

The unique pore structures encouraged us to examine the capacities of the two MOFs for gas adsorption. The low-pressure sorption isotherms of CO_2, C_2H_2, and C_2H_4 were collected at 273 and 296 K (Figure 2 and Figure S3 in the Supporting Information). At 296 K and 1 bar, **FJU-22a** can adsorb 111.3, 114.8, and 85.8 cm^3g^{-1} of CO_2, C_2H_2, and C_2H_4, respectively. The adsorption isotherms for C_2H_2, CO_2, and C_2H_4 on **FJU-21a** are very similar to those for **FJU-22a** and the adsorption capacity follows the same hierarchy: $C_2H_2 > CO_2 > C_2H_4$. This phenomenon may be attributed to the same pore surface structure resulting from the same metal node and ligand connection mode. However, the halved BET surface area for **FJU-21a** makes its various gas uptakes fall to half the corresponding values of **FJU-22a**. Furthermore, it is worth noting that the acetylene uptake isotherms for **FJU-21a** and **FJU-22a** at 296 K show a very sharp uptake at low pressure, whereas carbon dioxide uptake is much lower at this pressure. This discovery motivated us to examine their feasibility for the industrially important C_2H_2/CO_2 separation.

C_2H_2/CO_2 column breakthrough experiments

We first performed breakthrough simulations for a 50:50 (v/v) C_2H_2/CO_2 mixture on **FJU-21a** and **FJU-22a** by using the established methodology.[40] As shown in Figure S4 (in the Supporting Information), **FJU-21a** and **FJU-22a** are able to separate C_2H_2 from the C_2H_2/CO_2 mixture at room temperature. Clearly, **FJU-22a**, with good robustness, is more effective than **FJU-21a** for the C_2H_2/CO_2 separation. Thus, we only studied the actual performance of **FJU-22a** in the experimental column breakthrough.

In the actual column breakthrough experiment, an equimolar C_2H_2/CO_2 mixture was flowed over a packed column of the **FJU-22a** solid with a total flow of 5 $cm^3\,min^{-1}$ at 296 K (Figure 3). CO_2 was detected after the gas mixture has been introduced into the column for about 12 min, whereas C_2H_2 was not detected until a breakthrough time of 23 min was reached. Thus, the separation of C_2H_2/CO_2 mixture gases through a column packed with **FJU-22a** solid can be achieved efficiently. The breakthrough times of CO_2 and C_2H_2 on the unique

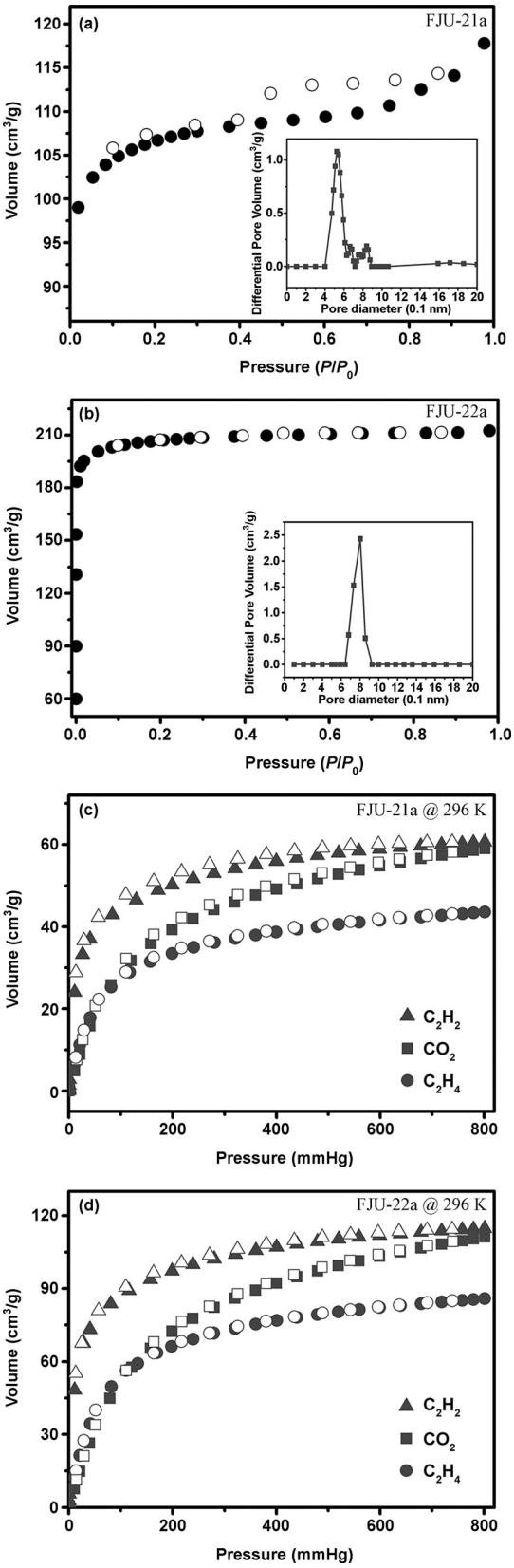

Figure 2. N_2 sorption isotherm and pore-size distributions at 77 K of **FJU-21a** (a) and **FJU-22a** (b). Adsorption isotherms for C_2H_2, CO_2, and C_2H_4 on **FJU-21a** (c) and **FJU-22a** (d) at 296 K (solid symbols: adsorption; open symbols: desorption).

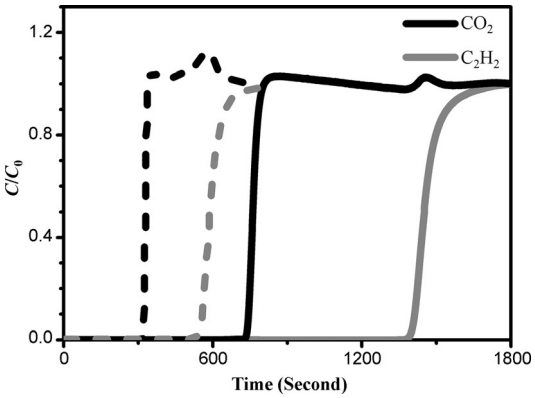

Figure 3. Experimental column breakthrough curve for an equimolar C_2H_2/CO_2 mixture in an adsorber bed packed with **FJU-22a** (——) or HOF-3a (-----) at ambient conditions (296 K, 1 bar). The total flow is of 5 $cm^3 min^{-1}$.

pore material HOF-3 were 5.5 and 9 min, respectively.[33] From the breakthrough curve, the separation selectivity, $\alpha = (q_1 y_2)/(y_1 q_2)$, for **FJU-22a** is 1.9, and close to 2.0 for HOF-3. However, **FJU-22a** has a separation capacity of 44.13 $cm^3 g^{-1}$, which is much higher than the value of 25.54 $cm^3 g^{-1}$ for HOF-3. At the same separation conditions, **FJU-22a**, with the open O donors, shows better performance than HOF-3, containing functional amino groups. **FJU-22a** is the first example of a MOF whose separation of a C_2H_2/CO_2 mixture has been clearly established by column breakthrough experiments.

First-principles calculations

To further understand the C_2H_2 and CO_2 adsorption on **FJU-22a**, detailed computational investigations were performed. We first optimized the bare **FJU-22a** structure by first-principles DFT-D (dispersion-corrected density-functional theory) calculations,[41] and then carried out Grand Canonical Monte Carlo (GCMC) simulations by using the classical force-field method. Based on the probability distribution of adsorbed gas molecules generated from the GCMC simulations, we introduced C_2H_2/CO_2 accordingly into the **FJU-22a** channel pore, and further optimized the structures by using DFT-D. We found that the guest molecules are associated with particular adsorption sites. Upon adsorption, both C_2H_2 and CO_2 sit right at the small cage connecting the two adjacent channel pores (Figure 4 and Figure S5 in the Supporting Information). Although the linker triazole ring has van der Waals (vdW) interactions with C_2H_2, the relatively strong binding between C_2H_2 and **FJU-22a** clearly comes from the hydrogen-bonding interactions between the C_2H_2 and the framework O ($d[O(\text{-}CO_2)\cdots H(C_2H_2)] = 2.290$ Å); this interaction does not exist between CO_2 and **FJU-22a** and CO_2 adsorption in the structure is mainly vdW-type in nature. The static C_2H_2 and CO_2 binding energies for **FJU-22a**, derived from the DFT-D calculations, are 33.3 and 22.6 kJ mol^{-1}, respectively. This difference in the gas/MOF framework interaction strength is likely the reason why the performance of separation for C_2H_2/CO_2 is outstanding in **FJU-22a** at room temperature.

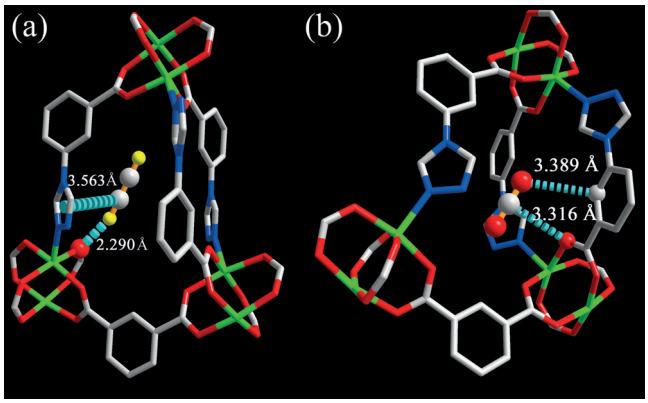

Figure 4. The C_2H_2 (a) and CO_2 (b) molecules sit right at the small cage connecting the two adjacent channel pores. Multiple-point interactions of the C_2H_2 with framework: *d*[O(-CO_2)···H(C_2H_2)] = 2.290 Å, *d*[center(-triazolyl)-···C(C_2H_2)] = 3.563 Å; multiple-point interactions between CO_2 molecule and the framework: *d*[O(-CO_2)···C(CO_2)] = 3.316 Å, *d*[C(-benzene)-···O(CO_2)] = 3.389 Å. Color code: Cu, green; C, gray; H, yellow; O, red; N, blue.

C_2H_2/C_2H_4 breakthrough experiments

The performance of **FJU-22a** for the removal of acetylene from C_2H_2/C_2H_4 mixtures containing 1% acetylene was examined through experimental column breakthrough in which a C_2H_2/C_2H_4 (1:99, v/v) mixture was flowed over a packed column of the **FJU-22a** solid with a total flow of 1.8 $cm^3 min^{-1}$ at 296 K. As shown in Figure 5, the separation of the C_2H_2/C_2H_4

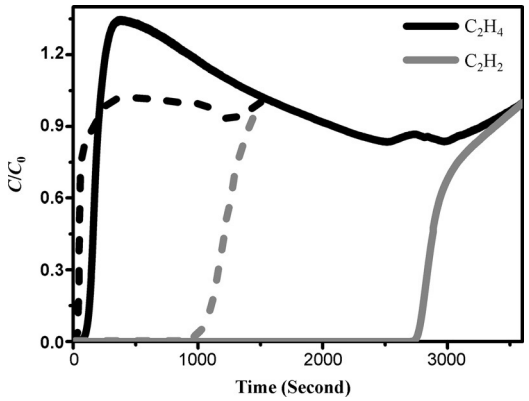

Figure 5. Experimental column breakthrough curve for an C_2H_2/C_2H_4 (1:99, v/v) mixture in an adsorber bed packed with **FJU-22a** (——) and UTSA-100a (-----) at ambient conditions (296 K, 1 bar). The total flows are 1.8 $cm^3 min^{-1}$ for **FJU-22**a and 2 $cm^3 min^{-1}$ for UTSA-100a.

mixture gases through a column packed with **FJU-22a** solid can be efficiently achieved, and the separation selectivity, α, for C_2H_2/C_2H_4 is 25.8. The adsorption and separation data for C_2H_2 and C_2H_4 gases on **FJU-22a** and some representative MOFs are given in Figure 6 and Table S4 (in the Supporting Information). M'MOF-3a, with a flexible framework, exhibits relative high separation selectivity (24.0), but very low acetylene uptakes, because of narrow pores and high sieving effects.[2] High densities of open metal sites can significantly endow the

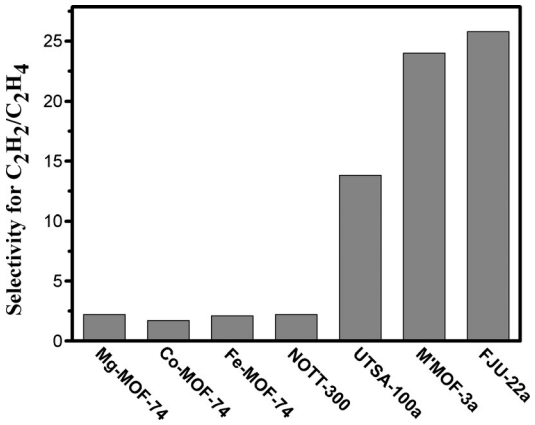

Figure 6. Selectivity for C_2H_2/C_2H_4 mixtures of some representative MOFs.

series of MOF-74 with high acetylene uptakes, but their selectivities for C_2H_2/C_2H_4 separation are systemically quite low[3] as the open metal sites have quite strong interactions toward both ethylene and acetylene molecules. NOTT-300 has multiple weak supramolecular interactions aligned within the host to form an optimal geometry for the selective binding of hydrocarbons, but the selectivity toward C_2H_2/C_2H_4 is still very low.[4] The multiple supramolecular interactions in NOTT-300 include the hydrogen-bonding interactions between C(C_2H_2 or C_2H_4) and H-O(framework), which are clearly distinct from those between O(framework) and H-C(C_2H_2) in **FJU-22a**. The former cannot recognize acetylene and ethylene very well, whereas the latter endows **FJU-22a** with exceptionally high selectivity. UTSA-100a,[5] containing amino groups with dual functionalities to simultaneously bind acetylene and sieve ethylene, has a relative high selectivity, about five times that for MOFs containing OMS. It is worth noting that **FJU-22** is isostructural with UTSA-100. The enthalpies of acetylene adsorption on both MOFs are almost same, but the separation selectivity, α, of **FJU-22a** is more than twice that for UTSA-100a, indicating that even in UTSA-100a (Figure S6 in the Supporting Information), the main contribution for its high selectivity toward acetylene may also come from the open O donor sites on the framework wall, rather than the amino groups. Conversely, the extra amino groups of UTSA-100a, to a certain extent, decrease its static C_2H_2 uptake. Despite its moderate static acetylene uptake, **FJU-22a** has the highest separation selectivity for the C_2H_2/C_2H_4 mixture among the reported porous materials. Based on the discussion above, open O donors on the pore wall can provide MOFs with better recognition for C_2H_2/C_2H_4 mixtures than the OMS and amino groups. **FJU-22a** is thus superior to the other MOFs, exhibiting highly efficient removal of acetylene from ethylene/acetylene mixtures containing 1% acetylene.

Conclusions

We have observed solvent-induced topological diversity enabling controllable robustness in two metal–organic frameworks (**FJU-21** and **FJU-22**) and have demonstrated that microporous

MOFs with open O sites are highly selective for the separation of C_2H_2/CO_2 and C_2H_2/C_2H_4 at ambient conditions. Control of the MOFs' robustness through tuning the helical chain SBUs is shown to be an efficient design approach for the first time. The good robustness of the activated **FJU-22a**, with open O donors, results in the extraordinary separation performance for mixtures of C_2H_2/CO_2 and C_2H_2/C_2H_4; this performance is superior to all the reported MOFs including the flexible **FJU-21a**. The separation capacity of **FJU-22a** for 50:50 C_2H_2/CO_2 mixtures is about twice that of HOF-3, the unique example for separation before our experiments. The actual selectivity of **FJU-22a** for C_2H_2/C_2H_4 mixtures containing 1% C_2H_2 is highest among the reported porous materials. Such preferential adsorption for C_2H_2 by **FJU-22a** rather than CO_2 and C_2H_4 is attributed to the open O donor sites on its framework wall. Open O donors can provide MOFs with better recognition ability for C_2H_2 than other functional sites, including open metal sites (OMS) and amino groups. It is expected that extensive research endeavors on porous MOFs will facilitate the discoveries of better C_2H_2 separation materials.

Experimental Section

General

All reagents and solvents were used as received from commercial suppliers without further purification. Thermogravimetric analyses (TGA) were performed with a Mettler Toledo TGA/SDTA851^e analyzer with a nitrogen flow and a heating rate of 10 K min^{-1} from 30 °C to 600 °C. Elemental analysis was collected with a Vario EL III elemental analyzer to give a ratio of C/H/N. Powder X-ray diffraction (PXRD) was carried out with a PANalytical X'Pert^3 powder diffractometer equipped with a Cu sealed tube ($\lambda = 1.54178$ Å) at 40 kV and 40 mA over the 2θ range 5–25°.

Synthesis

***N*,*N*-Dimethylformamide azine dihydrochloride (DMAz)**: The DMAz used in this study was synthesized by a modified version of the method in refs. [42,43]. Thionyl chloride ($SOCl_2$, 28.6 mL, 0.4 mol) was added with stirring to DMF (150 mL) at 5 °C. After addition, this mixture was kept at 5 °C for 24 h and then aqueous hydrazine hydrate (5 mL, 0.1 mol) in DMF (20 mL) was added slowly. After addition, the mixture was stirred at room temperature for 48 h and the white precipitate of *N*,*N*-dimethylformamide azine dihydrochloride was collected by filtration and washed with DMF and diethyl ether. Yield: 19.1 g; m.p.: 251 °C.

5-Triazole isophthalic acid (H_2L): A mixture of *N*,*N*-dimethylformamide azine dihydrochloride (4.0 g, 18.66 mmol) and 5-amino isophthalic acid (3.38 g, 18.66 mmol) was heated at reflux in 1,2-dimethylbenzene (50 mL) for 16 h to obtain a white solid. The solid was filtered and washed with ethanol (2×15 mL) and diethyl ether (1×17 mL). Yield: 1.62 g, 37.3%.

$\{[Cu(L)](DMF)(H_2O)_{1.5}\}_n$ (FJU-21): A mixture of CuI (0.1 mmol, 0.0191 g), H_2L (0.1 mmol, 0.0223 g), DMF (3 mL), and H_2O (2 mL) was stirred for 10 min. Then, the solution was transferred to a 23 mL glass reactor and heated to 85 °C. After 24 h, the system was cooled to room temperature and green needle-like crystals were obtained (32% yield with regard to H_2L). Elemental analysis calcd (%) for **FJU-21**: C 39.49, H 3.80, N 14.18; found: C 40.23, H 3.87, N 14.42.

$\{[Cu(L)]\cdot(DMA)(H_2O)_{1.5}\}_n$ (FJU-22): **FJU-22** was obtained by the same procedure used for preparation of **FJU-21** except that the DMF was replaced with DMA. Green bulk crystals of **FJU-22** were obtained (37% yield with regard to H_2L). Elemental analysis calcd (%) for **FJU-22**: C 41.08, H 4.16, N 13.69; found: C 41.78, H 4.21, N 14.05.

Single-crystal X-ray structure determination

Data collection and structural analysis of the crystals were collected on an Agilent Technologies SuperNova Single Crystal Diffractometer equipped with graphite monochromatic Cu K_α radiation ($\lambda = 1.54184$ Å). The crystal was kept at 293(10) K during data collection. Using Olex2,[44] the structure was solved with the Superflip structure solution program by using charge flipping and refined with the ShelXL refinement package by using least-squares minimization. The hydrogen atoms on the ligands were placed in idealized positions and refined by using a riding model. We employed PLATON[34]/SQUEEZE[35] to calculate the diffraction contribution of the solvent molecules in **FJU-21** and **FJU-22** and thereby produce a set of solvent-free diffraction intensities. The formulae of the crystals were calculated by elemental analysis. The detailed crystallographic data and structure refinement parameters for these compounds are summarized in the Supporting Information, Table S1. CCDC 1421052 (**FJU-21**) and 1421054 (**FJU-22**) contain the supplementary crystallographic data for this paper. These data are provided free of charge by The Cambridge Crystallographic Data Centre.

Gas adsorption measurements

A Micromeritics ASAP 2020 surface area analyzer was used to measure the gas adsorption. The sorption measurements were performed at 77 K with liquid nitrogen and at 273 K with an ice/water bath (slush). A water bath was used for adsorption isotherms at 296 K. DFT pore size distributions and pore sizes were calculated from the N_2 adsorption at 77 K.

Transient breakthrough simulations

The performance of industrial fixed-bed adsorbers is dictated by a combination of adsorption selectivity and uptake capacity. For a proper comparison of various MOFs, we performed transient breakthrough simulations by using the simulation methodology.[40] For the breakthrough simulations, the following parameter values were used: length of packed bed, $L = 0.3$ m; voidage of packed bed = 0.4; superficial gas velocity at inlet, $u = 0.04$ m s^{-1}. The framework density of **FJU-21** is 1104 kg m^{-3} and for **FJU-22** it is 1083 kg m^{-3}.

Column breakthrough test set-up, procedures, and measurements

The mixed-gas breakthrough separation experiment was conducted at 296 K by using a laboratory-scale fix-bed reactor. In a typical breakthrough experiment (Figure S7 in the Supporting Information) for the C_2H_2/CO_2 mixture, **FJU-22** powder (1.2 g) was packed into a quartz column (5.8 mm I.D.×150 mm) with silica wool filling the void space. The sorbent was activated in situ in the column with a vacuum pump at 333 K for 24 h. A helium flow (5 cm^3 min^{-1}) was introduced after the activation process to purge the adsorbent. The flow of He was then turned off while a gas mixture of C_2H_2/CO_2 (50:50, v/v) at 5 cm^3 min^{-1} was allowed to flow into the column. The effluent from the column was monitored by

using a mass spectrometer (MS). The absolute adsorbed amount of gas i (q_i) is calculated from the breakthrough curve by Equation (1):

$$q_i = \frac{F_i x t_0 - V_{dead} - \int_0^{t_0} F_e \Delta t}{m} \quad (1)$$

in which F_i is the influent flow rate of the specific gas ($cm^3 min^{-1}$), t_0 is the adsorption time (min), V_{dead} is the dead volume of the system (cm^3), F_e is the effluent flow rate of the specific gas ($cm^3 min^{-1}$), and m is the mass of the sorbent (g). The separation factor (α) of the breakthrough experiment is determined as:

$$\alpha = \frac{q_1 y_2}{y_1 q_2} \quad (2)$$

in which y_i is the molar fraction of gas i in the gas mixture. The column breakthrough measurement for C_2H_2/C_2H_4 (1:99, v/v) mixtures was similar to the measurements for the C_2H_2/CO_2 mixture, except that the helium flow was changed to 1.8 $cm^3 min^{-1}$.

Details of DFT-D calculations and GCMC simulations

First-principles calculations based on density-functional theory were performed by using the PWSCF package.[41] A semiempirical addition of dispersive forces to conventional DFT[45] was included in the calculation to account for van der Waals interactions. We used Vanderbilt-type ultrasoft pseudopotentials and the generalized gradient approximation (GGA) with the Perdew–Burke–Ernzerhof (PBE) exchange correlation. A cutoff energy of 544 eV and a $2\times2\times2$ k sampling were sufficient for the total energy to converge within 0.5 meV per atom. We first optimized the bare **FJU-22** structure. The optimized structure is fairly close to the experimental structure determined from XRD. C_2H_2 or CO_2 molecules were then introduced to the optimized HOF structure (guided by the GCMC result), followed by a full structural relaxation. To obtain the gas binding energies, a free gas molecule placed in a supercell with the same cell dimensions was also relaxed as a reference. The static binding energy was then calculated by using: $E_B = [E(MOF) + nE(gas) - E(MOF + ngas)]/n$. Grand Canonical Monte Carlo (GCMC) simulations[46] were performed for C_2H_2/CO_2 adsorption on **FJU-22**, with the gas molecules and the MOF frameworks both treated as rigid bodies. A $2\times2\times2$ supercell was used as the simulation box to ensure the simulation accuracy. A total of 2×10^7 steps were used for equilibration and an additional 2×10^7 steps were used to calculate the ensemble average of gas adsorption sites and thermodynamic properties. We used the standard universal force field (UFF)[47] to describe the gas–framework interaction and the gas–gas interaction. Atomic partial charges derived from first-principles calculations were included in the simulation to account for electrostatic interactions. The cut-off radius used for the Lennard–Jones interactions is 12.8 Å. The long-range electrostatic interactions were treated by using the Ewald summation technique with tin-foil boundary condition. Simulations were performed at various temperatures and pressures. The probability distributions of adsorbed C_2H_2 and CO_2 were generated from the simulation after the equilibrium stage.

Acknowledgments

This work was financially supported by the National Natural Science Foundation of China (21207018, 21273033, 21203024, and 21573042) and the Fujian Science and Technology Department (2014J06003 and 2014H6007). S.X. gratefully acknowledges the support of the Recruitment Program of Global Young Experts, Program for New Century Excellent Talents in University (NCET-10-0108), and the Award 'MinJiang Scholar Program' in Fujian Province.

Keywords: column breakthrough · metal–organic frameworks · open O donors · selective gas adsorption · structural diversity

[1] F. Studt, F. Abild-Pedersen, T. Bligaard, R. Z. Sørensen, C. H. Christensen, J. K. Nøskov, *Science* **2008**, *320*, 1320–1322.
[2] S. C. Xiang, Z. J. Zhang, C. G. Zhao, K. L. Hong, X. B. Zhao, D. R. Ding, M. H. Xia, C. D. Wu, M. C. Das, R. Gill, K. M. Tomoas, B. L. Chen, *Nat. Commun.* **2011**, *2*, 204.
[3] a) E. D. Bloch, W. L. Queen, R. Krishna, J. M. Zadrozny, C. M. Brown, J. R. Long, *Science* **2012**, *335*, 1606–1610; b) Y. B. He, R. Krishna, B. L. Chen, *Energy Environ. Sci.* **2012**, *5*, 9107–9120.
[4] S. H. Yang, A. J. Ramirez-Cuesta, R. Newby, V. Garcia-Sakai, P. Manuel, S. K. Callear, S. I. Campbell, C. C. Tang, M. Schröder, *Nat. Chem.* **2014**, *7*, 121–129.
[5] T. L. Hu, H. L. Wang, B. Li, R. Krishna, H. Wu, W. Zhou, Y. F. Zhao, Y. Han, X. Wang, W. D. Zhu, Z. Z. Yao, S. C. Xiang, B. L. Chen, *Nat. Commun.* **2015**, *6*, 7328.
[6] B. M. Collins, US Patent 4126645, **1978**.
[7] W. Huang, J. R. McCormick, R. F. Lobo, J. G. Chen, *J. Catal.* **2007**, *246*, 40–51.
[8] a) B. M. Choudary, M. Lakshmi Kantam, N. Mahender Reddy, K. Koteswara Rao, Y. Haritha, V. Bhaskar, F. Figueras, A. Tuel, *Appl. Catal. A* **1999**, *181*, 139–144; b) N. A. Khan, S. Shaikhutdinov, H. J. Freund, *Catal. Lett.* **2006**, *108*, 159–164.
[9] K. Weissermel, H. J. Arpe, *Industrial Organic Chemistry*, 4th ed., 91–98, Wiley-VCH, Weinheim, **2003**.
[10] a) H. Furukawa, K. E. Cordova, M. O'Keeffe, O. M. Yaghi, *Science* **2013**, *341*, 1230444; b) J. R. Long, O. M. Yaghi, *Chem. Soc. Rev.* **2009**, *38*, 1213–1214.
[11] a) H. C. Zhou, S. Kitagawa, *Chem. Soc. Rev.* **2014**, *43*, 5415–5418; b) H. Sato, W. Kosaka, R. Matsuda, A. Hori, Y. Hijikata, R. V. Belosludov, S. Sakaki, M. Takata, S. Kitagawa, *Science* **2014**, *343*, 167–170.
[12] G. Férey, C. Serre, *Chem. Soc. Rev.* **2009**, *38*, 1380–1399.
[13] a) S. J. Bao, R. Krishna, Y. B. He, J. S. Qin, Z. M. Su, S. L. Li, W. Xie, D. Y. Du, W. W. He, S. R. Zhang, Y. Q. Lan, *J. Mater. Chem. A* **2015**, *3*, 7361–7367; b) S. L. Li, Y. Q. Lan, H. Sakurai, Q. Xu, *Chem. Eur. J.* **2012**, *18*, 16302–16309; c) Q. L. Zhu, Q. Xu, *Chem. Soc. Rev.* **2014**, *43*, 5468–5512; d) J. K. Sun, Q. Xu, *Energy Environ. Sci.* **2014**, *7*, 2071–2100; e) J. S. Li, Y. J. Tang, S. L. Li, S. R. Zhang, Z. H. Dai, Z. H. Si, Y. Q. Lan, *CrystEngComm* **2015**, *17*, 1080–1085; f) D. Y. Du, J. S. Qin, S. L. Li, Z. M. Su, Y. Q. Lan, *Chem. Soc. Rev.* **2014**, *43*, 4615–4632.
[14] R. Matsuda, R. Kitaura, S. Kitagawa, Y. Kubota, R. V. Belosludov, T. C. Kobayashi, H. Sakamoto, T. M. Takata, Y. Kawazoe, T. Chiba, Y. Mita, *Nature* **2005**, *436*, 238–241.
[15] a) J. B. Lin, W. Xue, J. P. Zhang, X. M. Chen, *Chem. Commun.* **2011**, *47*, 926–928; b) P. Q. Liao, H. Y. Chen, D. D. Zhou, S. Y. Liu, C. T. He, Z. B. Rui, H. B. Ji, J. P. Zhang, X. M. Chen, *Energy Environ. Sci.* **2015**, *8*, 1011–1016.
[16] a) A. Samanta, A. Zhao, G. K. H. Shimizu, P. Sarkar, R. Gupta, *Ind. Eng. Chem. Res.* **2012**, *51*, 1438–1463; b) R. Vaidhyanathan, S. S. Iremonger, G. K. H. Shimizu, P. G. Boyd, S. Alavi, T. K. Woo, *Angew. Chem. Int. Ed.* **2012**, *51*, 1826–1829; *Angew. Chem.* **2012**, *124*, 1862–1865; c) R. Vaidhyanathan, S. S. Iremonger, K. W. Dawsona, G. K. H. Shimizu, *Chem. Commun.* **2009**, 5230–5232.

[17] a) X. Zhao, X. H. Bu, Q. G. Zhai, H. Tran, P. Y. Feng, *J. Am. Chem. Soc.* **2015**, *137*, 1396 – 1399; b) Q. G. Zhai, Q. Lin, T. Wu, L. Wang, S. T. Zheng, X. H. Bu, P. Y. Feng, *Chem. Mater.* **2012**, *24*, 2624 – 2626; c) Q. Lin, T. Wu, S. T. Zheng, X. H. Bu, P. Y. Feng, *J. Am. Chem. Soc.* **2012**, *134*, 784 – 787.

[18] a) J. G. Duan, W. Q. Jin, R. Krishna, *Inorg. Chem.* **2015**, *54*, 4279 – 4284; b) Y. P. Chen, Y. Y. Liu, D. H. Liu, M. Bosch, H. C. Zhou, *J. Am. Chem. Soc.* **2015**, *137*, 2919 – 2930; c) C. Wang, D. M. Liu, W. B. Lin, *J. Am. Chem. Soc.* **2013**, *135*, 13222 – 13234; d) W. J. Wang, D. Q. Yuan, *Sci. Rep.* **2014**, *4*, 5711.

[19] a) J. Y. Lee, L. Pan, X. Y. Huang, T. J. Emge, J. Li, *Adv. Funct. Mater.* **2011**, *21*, 993 – 998; b) H. Liu, Y. G. Zhao, Z. J. Zhang, N. Nijem, Y. J. Chabal, H. P. Zeng, J. Li, *Adv. Funct. Mater.* **2011**, *21*, 4754 – 4762; c) Y. Chen, H. Wang, J. Li, J. V. Lockard, *J. Mater. Chem. A J. Mater. Chem. A.* **2015**, *3*, 4945 – 4953; d) H. Wang, K. Yao, Z. Zhang, J. Jagiello, Q. Gong, Y. Han, J. Li, *Chem. Sci.* **2014**, *5*, 620 – 624.

[20] a) X. Duan, J. F. Cai, J. C. Yu, C. D. Wu, Y. J. Cui, Y. Yang, G. D. Qian, *Microporous Mesoporous Mater.* **2013**, *181*, 99 – 104; b) T. F. Xia, J. F. Cai, H. Z. Wang, X. Duan, Y. J. Cui, Y. Yang, G. D. Qian, *Microporous Mesoporous Mater.* **2015**, *215*, 109 – 115.

[21] M. Fischer, F. Hoffmann, M. Froeba, *ChemPhysChem* **2010**, *11*, 2220 – 2229.

[22] J. W. Yoon, J. S. Lee, S. Lee, K. H. Cho, Y. K. Hwang, M. Daturi, C. H. Jun, R. Krishna, J. S. Chang, *Chem. Eur. J* **2015**, *50*, 18431 – 18438.

[23] H. M. Wen, B. Li, H. L. Wang, R. Krishna, B. L. Chen, *Chem. Commun.* **2016**, *52*, 1166 – 1169.

[24] Y. B. He, S. C. Xiang, B. L. Chen, *J. Am. Chem. Soc.* **2011**, *133*, 14570 – 14573.

[25] M. C. Das, Q. S. Guo, Y. B. He, J. Kim, C. G. Zhao, K. Hong, S. C. Xiang, Z. J. Zhang, K. M. Thomas, R. Krishna, B. L. Chen, *J. Am. Chem. Soc.* **2012**, *134*, 8703 – 8710.

[26] S. J. Lee, J. W. Yoon, Y. K. Seo, M. B. Kim, S. K. Lee, U. H. Lee, Y. K. Hwang, Y. S. Bae, J. S. Chang, *Microporous Mesoporous Mater.* **2014**, *193*, 160 – 165.

[27] H. M. Wen, B. Li, H. L. Wang, C. Wu, K. Alfooty, R. Krishnad, B. L. Chen, *Chem. Commun.* **2015**, *51*, 5610 – 5613.

[28] Z. J. Zhang, S. C. Xiang, B. L. Chen, *CrystEngComm* **2011**, *13*, 5983 – 5992.

[29] a) Z. J. Zhang, Z. Z. Yao, S. C. Xiang, B. L. Chen, *Energy Environ. Sci.* **2014**, *7*, 2868 – 2899; <lit b> S. C. Xiang, Y. B. He, Z. J. Zhang, H. Wu, W. Zhou, R. Krishna, B. L. Chen, *Nat. Commun.* **2012**, *3*, 954.

[30] a) S. C. Xiang, W. Zhou, Z. J. Zhang, M. A. Green, Y. Liu, B. L. Chen, *Angew. Chem. Int. Ed.* **2010**, *49*, 4615 – 4618; *Angew. Chem.* **2010**, *122*, 4719 – 4722; b) S. C. Xiang, W. Zhou, J. M. Gallegos, Y. Liu, B. L. Chen, *J. Am. Chem. Soc.* **2009**, *131*, 12415 – 12419; c) C. L. Song, J. Y. Hu, Y. J. Ling, Y. L. Feng, D. L. Chen, Y. B. He, *Dalton Trans.* **2015**, *44*, 14823 – 14829.

[31] J. D. Pang, F. L. Jiang, M. Y. Wu, C. P. Liu, K. Z. Su, W. G. Lu, D. Q. Yuan, M. C. Hong, *Nat. Commun.* **2015**, *6*, 7575.

[32] a) Y. B. He, S. C. Xiang, Z. J. Zhang, S. S. Xiong, F. R. Fronczek, R. Krishna, M. O'Keeffe, B. L. Chen, *Chem. Commun.* **2012**, *48*, 10856 – 10858; b) H. Xu, Y. B. He, Z. J. Zhang, S. C. Xiang, J. F. Cai, Y. J. Cui, Y. Yang, G. D. Qian, B. L. Chen, *J. Mater. Chem. A* **2013**, *1*, 77 – 81; c) J. P. Zhang, X. M. Chen, *J. Am. Chem. Soc.* **2009**, *131*, 5516 – 5521; d) M. Bülow, C. J. Guo, D. G. Shen, F. R. Fitch, A. I. Shirley, A. I. L. Cava, J. P. Brooks, US Patent 6024781, **2000**.

[33] P. Li, Y. B. He, Y. F. Zhao, L. H. Weng, H. L. Wang, R. Krishna, H. Wu, W. Zhou, M. O'Keeffe, Y. Han, B. L. Chen, *Angew. Chem. Int. Ed.* **2015**, *54*, 574 – 577; *Angew. Chem.* **2015**, *127*, 584 – 587.

[34] A. L. Speka, *J. Appl. Crystallogr.* **2003**, *36*, 7 – 13.

[35] A. L. Spek, *Acta Crystallogr. Sect. A* **1990**, *46*, C34.

[36] a) H. Chevreau, T. Devic, F. Salles, G. Maurin, N. Stock, C. Serre, *Angew. Chem. Int. Ed.* **2013**, *52*, 5056 – 5060; *Angew. Chem.* **2013**, *125*, 5160 – 5164; b) L. Valenzano, B. Civalleri, S. Chavan, *Chem. Mater.* **2011**, *23*, 1700 – 1718.

[37] A. Schaate, P. Roy, A. Godt, J. Lippke, F. Waltz, M. Wiebcke, P. Behrens, *Chem. Eur. J.* **2011**, *17*, 6643 – 6651.

[38] V. Colombo, S. Galli, H. J. Choi, G. D. Han, A. Maspero, G. Palmisano, N. Masciocchic, J. R. Long, *Chem. Sci.* **2011**, *2*, 1311 – 1319.

[39] C. Yang, U. Kaipa, Q. Z. Mather, X. P. Wang, V. Nesterov, A. F. Venero, M. A. Omary, *J. Am. Chem. Soc.* **2011**, *133*, 18094 – 18097.

[40] R. Krishna, *RSC Adv.* **2015**, *5*, 52269 – 52295.

[41] P. Giannozzi, S. Baroni, N. Bonini, M. Calandra, R. Car, C. Cavazzoni, D. Ceresoli, G. L. Chiarotti, M. Cococcioni, I. Dabo, A. Dal Corso, S. Fabris, G. Fratesi, S. de Gironcoli, R. Gebauer, U. Gerstmann, C. Gougoussis, A. Kokalj, M. Lazzeri, L. Martin-Samos, N. Marzari, F. Mauri, R. Mazzarello, S. Paolini, A. Pasquarello, L. Paulatto, C. Sbraccia, S. Scandolo, G. Sclauzero, A. P. Seitsonen, A. Smogunov, P. Umari, R. M. Wentzcovitch, *J. Phys. Condens. Matter* **2009**, *21*, 395502.

[42] T. Panda, T. Kundu, R. Banerjee, *Chem. Commun.* **2012**, *48*, 5464 – 5466.

[43] L. Wen, W. Shi, X. T. Chen, H. H. Li, P. Cheng, *Eur. J. Inorg. Chem.* **2012**, *22*, 3562 – 3568.

[44] a) G. M. Sheldrick, *Acta Crystallogr. Sect. A* **2008**, *64*, 112 – 122; b) A. V. Dolomanov, L. J. Bourhis, R. J. Gildea, J. A. K. Howard, H. Puschmann, *J. Appl. Crystallogr.* **2009**, *42*, 339 – 341.

[45] V. Barone, M. Casarin, D. Forrer, M. Pavone, M. Sambi, A. J. Vittadini, *Comput. Chem.* **2009**, *30*, 934 – 939.

[46] D. Frenkel, B. Smit, *Computational Science Series*, Academic Press, San Diego, **2002**.

[47] A. K. Rappe, C. J. Casewit, K. S. Colwell, W. A. Goddard III, W. M. Skid, *J. Am. Chem. Soc.* **1992**, *114*, 10024 – 10035.

Received: December 21, 2015
Published online on March 2, 2016